Abyssal Stratification Change in the Southwest Pacific Basin

Helen. J. Zhang[1], Caitlin. B. Whalen[1], Nirnimesh Kumar[2], Sarah. G. Purkey[3]

[1]Applied Physics Laboratory, University of Washington
[2]Civil and Environmental Engineering, University of Washington
[3]Scripps Institution of Oceanography, University of California, San Diego

Key Points:

- A decadal stratification decrease estimated from 25 years of repeat hydrography is observed in the abyssal Southwest Pacific Basin
- This change is significant below $\Theta = 0.75$ °C and intensifies with depth to a per decade scaling factor of 0.71 ± 0.07 by $\Theta = 0.65$ °C
- Vertical diffusive heat flux is also reduced during the same time period by about 0.01 Wm^{-2}/decade

Corresponding author: H.J Zhang, hjzhang@uw.edu

Abstract

As abyssal ocean properties are altered by climate change, density stratification may be expected to change in response. This shift can affect the buoyancy flux, internal wave generation, and turbulent dissipation, which may impact mixing and vertical transport. In this study, repeated surveys of three hydrographic sections in the Southwest Pacific Basin between the 1990s-2010s are used to estimate the change in buoyancy frequency N^2. We find that below $\Theta = 0.8$ °C, N^2 is reduced by a mean scaling factor of 0.88± 0.06 per decade. This reduction is intensified at depth, with the biggest change observed at $\Theta = 0.63$ °C by a scaling factor of 0.71 ± 0.07 . Within the same time period, the magnitude of per unit area vertical diffusive heat flux is reduced by about 0.01 Wm^{-2}, although this estimate is sensitive to the choice of estimated diffusivity. Finally, implications on heat budget and global ocean circulation are qualitatively discussed.

Plain Language Summary

Since the 1990s, the coldest water mass, which originates off Antarctica and fills most of the world's deepest ocean basins, has warmed significantly. Since cold water is denser and heavier, this observed warming has caused the deepest ocean water to lighten, altering the vertical structure of the water column. Using repeated ship-based measurements of temperature, salinity, and pressure, we find a weakening vertical density gradient in the very deep Southwest Pacific Basin between the 1990s-2010s. As a result, water near the seafloor became more homogeneous. This impacts the water's buoyancy and reduces the deep ocean's ability to mix in heat from above. Since large scale currents in the deep ocean are primarily driven by density differences and vertical mixing, the observed change may impact the global ocean circulation. This can have implications for deep ocean heat storage and future climate projections.

1 Introduction

Since the 1950s, more than 90% of the observed warming on Earth has occurred in the ocean, with one-third of the heat uptake going into waters below 4000 m (Purkey & Johnson, 2010; D. G. Desbruyères et al., 2016). Increased glacial melting has also produced a flux of freshwater off Antarctica and into the Southern Ocean (Jacobs & Giulivi, 2010; Purkey & Johnson, 2013; Rignot et al., 2019). This local warming and freshening

is transported globally via the Meridional Overturning Circulation (hereinafter MOC). The MOC is a balance between the renewal of cold water and diapycnal mixing of heat, therefore it is sensitive to changes in water temperature and salinity, which can affect its overall heat and volume transport (Munk, 1966; Lumpkin & Speer, 2007). Since the 1990s, numerous studies have noted a contraction of abyssal northward flow, the bottom branch of the MOC (Johnson et al., 2008; Kouketsu et al., 2009; Purkey & Johnson, 2012). Large scale shifts in temperature and salinity can change the structure of the water column by altering the vertical density gradient, or stratification. This has implications for abyssal upwelling, which sets the strength of the MOC (Talley et al., 2003; Lumpkin & Speer, 2007). However, no observational studies to our knowledge have focused on the role of changing climate on the strength of deep ocean stratification.

Past analysis of global temperature and salinity have shown that their changes are non-uniform throughout the water column, with a local maximum in warming and freshening observed along the pathway of Antarctic Bottom Water (AABW) (Purkey & Johnson, 2010; Kouketsu et al., 2011; Purkey & Johnson, 2013; D. Desbruyères et al., 2017). This dense water mass is formed from cold and saline water off Antarctica in the Ross Sea and along the Adelie Coast, sinking down the continental slope and flowing northward along deep western boundary currents (DWBC) (Orsi et al., 1999; Talley, 2013). As AABW travels north, diapycnal mixing brings in heat from above, lightening the bottom water and driving upwelling (Munk, 1966; Lumpkin & Speer, 2007). This process ventilates the abyssal ocean forming the upwards branch of the overturning circulation (Nikurashin & Ferrari, 2013; De Lavergne et al., 2016). As a consequence, this bottom water is newer than the deep waters above (England, 1995). Due to Antarctica's accelerated warming and freshening from melt-water, AABW production has slowed significantly (Purkey & Johnson, 2012; Jacobs & Giulivi, 2010), although salinity in some source regions have rebounded in the last decade (Castagno et al., 2019). While the time scale of the MOC is multi-centennial, models have shown that the warm anomaly from changes in deep water production rate can propagate from the Adelie Coast to the North Pacific in as little as 40 years (Masuda et al., 2010). Therefore, recent climate changes near Antarctica can have a global effect on timescales within a few decades, and fingerprints of these changes can be observed in the time-span of global data collection (Johnson et al., 2007; Purkey & Johnson, 2010).

Stratification change affects the medium of local dynamics, which can have feedback effects on global climate. For example, this change can affect the generation of internal waves due to barotropic tidal flow over uneven topography (Bell, 1975; Baines, 1982; Garrett & Kunze, 2007). Globally, the tides input about 1 TW into the internal wave field, a significant portion of the total mixing required to close the MOC (Egbert & Ray, 2000; St. Laurent & Simmons, 2006; Waterhouse et al., 2014). Once internal waves are generated, stratification also affect their propagation, breaking, and subsequent turbulent dissipation (Gregg, 1989). Finally, it directly impacts the temperature gradient, which sets the vertical heat flux. Through multiple ways, stratification is linked to the vertical transport of water and heat, a key aspect of climate projections (Melet, Hallberg, et al., 2013; Melet et al., 2014).

While the processes discussed above are global, it is valuable to analyze their exact mechanisms on a sub-basin scale. This paper focuses on the Southwest Pacific Basin, a key pathway in the transport of AABW (Fig. 1) that connects deep waters in the Southern Ocean to the Pacific (Whitworth et al., 1999; Sloyan & Rintoul, 2001). As there is no deep water formation in the North Pacific, the bottom branch of the Pacific MOC is sourced exclusively from southern high latitudes and carried north via the DWBC. In the southern subtropical latitudes, despite mixing by the Antarctic Circumpolar Current, more than 70% of the water in the abyssal ocean is AABW in origin (Johnson, 2008). AABW is carried into the basin south of the Campbell Plateau, flowing northwards through the Kermadec and Tonga Trench, and exiting into the Pacific Basin via the Samoan Passage (Fig. 1). In the Samoan Passage, most of the northward flow is below 0.85 °C (Roemmich et al., 1996; Voet et al., 2016). Since AABW warms as it travels north, within the scope of this paper, we shall define AABW to be everything colder than 0.8 °C.

Here we quantify the stratification change in the Southwest Pacific Basin from the 1990s through 2017 and analyze the spatial pattern. Basin wide averages of the change in both stratification and heat flux are estimated. Finally, we discuss the implications and potential feedbacks.

2 Data and Methods

In this study, we use deep ocean temperature, salinity, and pressure data from repeated ship-based hydrographic surveys to determine the decadal rate of change of sec-

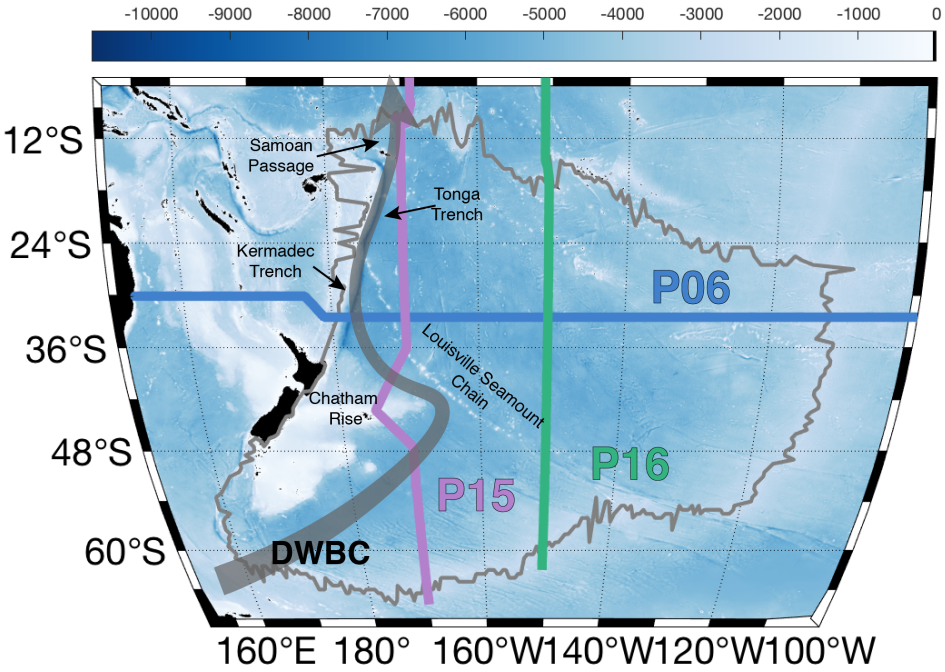

Figure 1. A map of the Southwest Pacific Basin bathymetry. The grey outline indicates the basin boundary (Purkey & Johnson, 2010). WOCE sections considered in this analysis are depicted, and key topographical features are labeled for reference. The grey arrow represents the approximate pathway of the Deep Western Boundary Current (Whitworth et al., 1999).

ond order characteristics in the abyssal Southwest Pacific Basin. This data is first collected in the 1990s by the World Ocean Circulation Experiment (WOCE), which conducted full-depth high resolution CTD surveys along sections transecting the world's oceans. This effort is sustained through the 2000s and 2010s by the Climate Variability and Predictability (CLIVAR) program, and currently by the Global Ocean-Based Hydrographic Investigations Program (GO-SHIP).

We consider a latitudinal section, P06, and two longitudinal sections P15 and P16 (Fig. 1). P06 (blue line) provides a zonal cross section of northward bottom water transport while P15 and P16 (purple and green lines) capture a meridional view. P06 was occupied in 1992, 2003, 2010, and 2017, P15 in 1996, 2001, 2009, and 2016, and P16 in 1992, 2005, and 2014. CTD samples are nominally spaced 55 km apart. Temperature and salinity observations are made from the surface to within 10-20 m of the seafloor and initially binned into 1 or 2 dbar pressure grids. The instrumental accuracy for temperature, salinity, and pressure profiles are $\pm 0.002°$C, ± 0.002 PSS-78, and ± 3 dbar respectively (Hood et al., 2010). For more accurate salinity comparisons between occupations, batch-to-batch salinity offsets are applied following Kawano et al. (2006).

The quality controlled temperature, salinity, and pressure data are used to calculate absolute salinity (S_A) and conservative temperature (Θ), the parameters of the TEOS-10 toolbox used throughout the analysis (McDougall & Barker, 2011). Following the methods of Purkey and Johnson (2010), a 40-dbar half-width Hanning filter is applied to each S_A and Θ profile, which is then interpolated onto a vertical 40 dbar pressure grid. This coarser grid was chosen to minimize noise from transient eddies in the data in favor of large scale changes. In each pressure bin, the data is then interpolated onto a $2°$ latitude or longitude horizontal grid selected to encompass the most overlap between each occupation. The maximum pressure of each profile is taken to be the seafloor depth, and used to mask over any interpolated data.

We define stratification as the square of buoyancy frequency, N^2. This is calculated for each grid point using,

$$N^2 = g^2 \, \frac{\beta \Delta S_A - \alpha \Delta \Theta}{V_{sp} \, \Delta P} \tag{1}$$

where dS_A and $d\Theta$ is the difference between the value at a given pressure bin with the one above, α and β are the thermal expansion and saline contraction coefficients respec-

tively, V_{sp} is the specific volume calculated using a 75-term polynomial expression, and P is pressure in Pascals (Roquet et al., 2015).

For each grid point, we also calculate vertical heat flux (Q) using the equation,

$$Q = \rho c_p \kappa N^2_\Theta \tag{2}$$

where ρ and c_p are the density and heat capacity of seawater, both constants in this analysis. N^2_Θ is the vertical gradient of conservative temperature, or $\frac{\partial}{\partial z}\Theta$. The diffusivity κ, is parameterized in two different ways. The first is the canonical constant value 10^{-4} m^2/s, so that heat flux is proportional N^2_Θ (Munk, 1966; Waterhouse et al., 2014). The second is a gridded spatially variable diffusivity calculated using an average of the finescale parameterization derived from N^2 strain calculated for each occupation (K. L. Polzin et al., 1995; Whalen et al., 2015). Since processing choices made in early occupations influence the data fine structure, we only use parameterized diffusivities from occupations after 1995. Furthermore, as diffusivity is a log-normal variable, a geometric mean is used to estimate the average value (Gurvich & Yaglom, 1967; Gregg, 1989).

2.1 Isotherm Grid

The gridded N^2 and heat flux are reparameterized by density to eliminate effects from isopycnal heave. Since salinity errors have a more significant impact on density, especially in the deep ocean, temperature is chosen as the independent variable (Purkey & Johnson, 2013). Using Θ from each occupation, the pressure binned values are piecewise cubic interpolated onto a 0.01°C grid. In this framework, each vertical bin represents a single temperature class. As we define AABW by temperature, this reparameterization allows for comparisons between the water mass' properties over time, regardless of its vertical movement in the water column.

2.2 Change over Time

The change in N^2 or heat flux over time is estimated using a linear fit across all occupations of each section. Since the sections are re-occupied about once every decade, changes are estimated on a decadal scale. To further minimize small scale fluctuations with depth, we average the value of each bin with that of the bins above and below (except along boundaries) prior to taking the fit.

Since N^2 is a log-normal value (Gregg, 1989), we perform the linear fit on $\log(N^2)$. By comparing the order of magnitude of N^2, rather than its absolute value, $\frac{\partial}{\partial t}$ is an expression for the relative change over time. Thus, $\frac{\partial}{\partial t}\log(N^2)$ is better expressed as a scaling factor, defined as

$$s(N^2) = 10^{\frac{\partial}{\partial t}\log(N^2)} \tag{3}$$

For example, $\frac{\partial}{\partial t}\log(N^2) = -0.1$ is equivalent to a factor of $s = 0.8$. Hence, every decade N^2 is scaled by 0.8, or a 20% decrease. Using this method for all grid points, we produce a gridded map of $s(N^2)$ for each section.

The data for P15 is different: only the first and last occupation sampled latitudes south of 47.5°S. Change in this region is calculated separately based on the two occupations.

2.3 Basin Averages and Errors

We estimate change in the total basin by calculating the length weighted mean and standard deviation of all three sections. The study region is constrained within the boundaries of the Southwest Pacific Basin as defined by Purkey and Johnson (2010).

Confidence intervals are determined by calculating the degree of freedom (DOF) of each temperature class, obtained by dividing the length of that isotherm by a horizontal decorrelation length scale of 163 km (Purkey & Johnson, 2010). If the isotherm is segmented by topography, each portion is assumed to be statistically independent and contribute at least one DOF. The standard error is estimated by dividing the standard deviation by the square root of the DOF. The 95% confidence interval is estimated using a Student's t distribution.

3 Results

Warming between 1990s-2010s is more prominent near the bottom, a trend which has been observed in all three sections in this analysis and noted by multiple previous studies (Purkey & Johnson, 2010; Sloyan et al., 2013; D. G. Desbruyères et al., 2016). This warming is primarily observed below $\Theta = 0.8$ °C, so that isotherms below this boundary grow further apart. Since salinity effects are small, the increasing separation of isotherms manifests as a reduction of stratification.

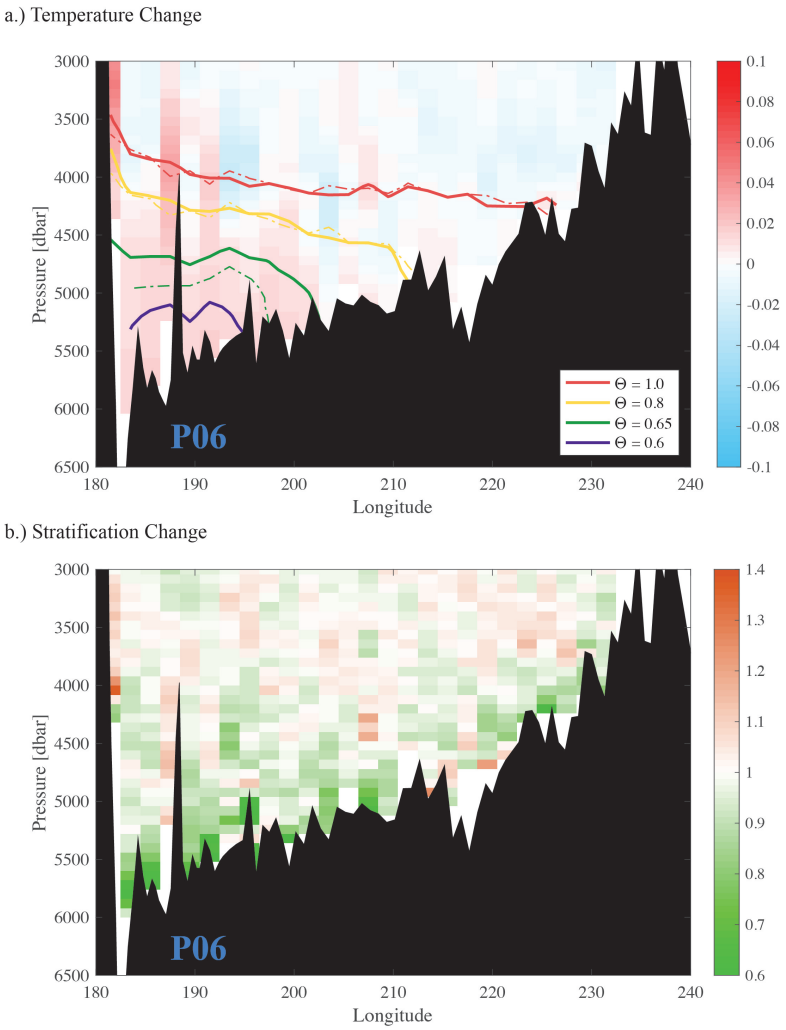

Figure 2. Decadal rate of change of conservative temperature $d\Theta/dt$ along section P06 within the basin. Warming regions are shaded in red while cooling regions are shaded blue. Contoured isotherms from 1992 (solid line) and 2017 (dashed line) are depicted. (b) Decadal fractional change of the Brunt Väisälä frequency N^2. Decreasing N^2 is shaded green, increasing N^2 shaded orange. The seafloor is masked over in black.

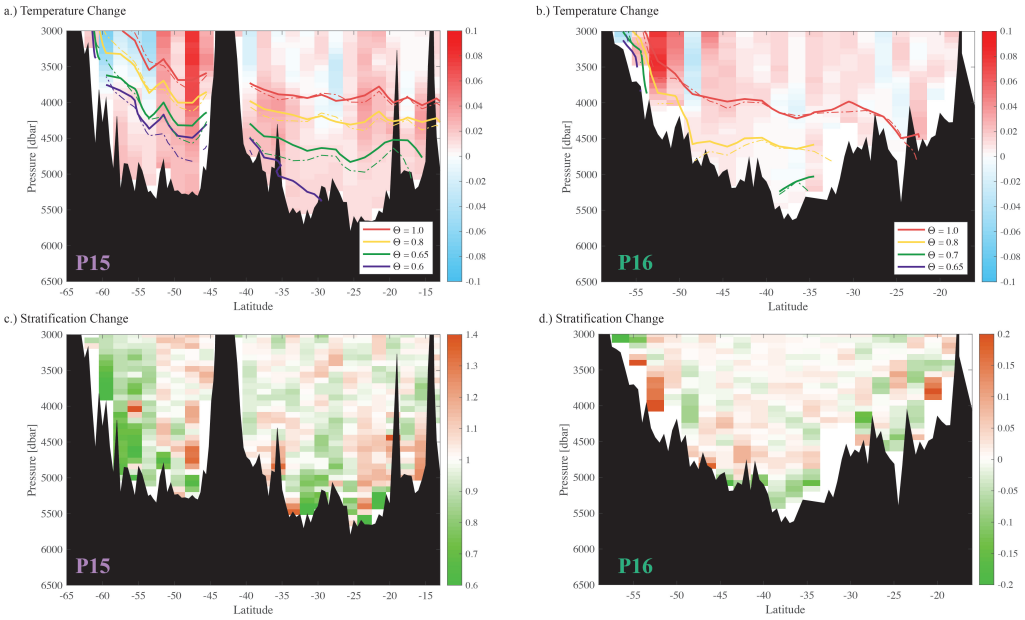

Figure 3. Decadal conservative temperature rate of change (a-b) and N^2 fractional change (c-d) along sections P15 and P16 following Fig. 2

The average decadal warming below $\Theta = 1.0$ °C section P06 is of $\mathcal{O}(10^{-3})$ °C (Fig. 2 a). This is an order of magnitude greater than the average observed warming above $\Theta = 0.8$ °C and below $\Theta = 1.0$ °C. Abyssal warming is most prominent in the western side of the basin along the path of the DWBC (Fig. 2a). Within the AABW, warming is strongest near the sea floor. As a result, colder isotherms deeper in the water column have fallen at a faster rate. Between 1992 and 2017, the $\Theta = 0.65$ °C isotherm has fallen by 562.25 m, while the $\Theta = 0.8$ °C isotherm only fell by 14.17 m. Further down the water column, the $\Theta = 0.6$ °C isotherm has completely disappeared by 2017, indicating an absence of the coldest waters. In contrast, warmer isotherms such as $\Theta = 1.0$ °C have remained relatively stationary due to minimal temperature changes.

Another consequence of changing bottom water properties is a reduction of near bottom stratification (Fig. 2b). The stratification change over time $\frac{\partial}{\partial t}N^2$ is concentrated along the seafloor. The biggest decrease is observed in the Kermadec Trench around 183°, where N^2 has dropped by approximately 40% per decade. Both $\frac{\partial}{\partial t}\Theta$ and $\frac{\partial}{\partial t}N^2$ show a stronger warming/reduction on the western side of the basin, which is spatially consistent with the path of AABW as it flows northward with the DWBC (Fig. 1). On the eastern side, a smaller N^2 reduction is observed along the East Pacific Rise.

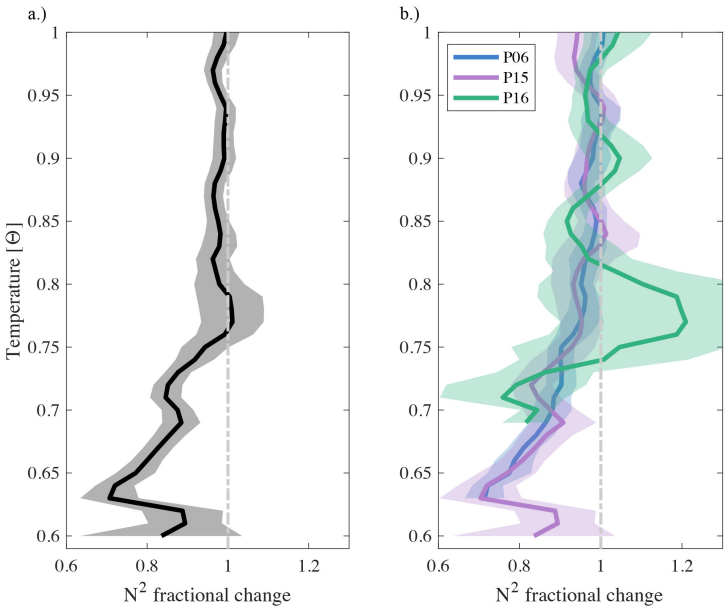

Figure 4. Average decadal N^2 fraction change in conservative temperature coordinates (a) weighted by length for all basin sections (b) for each section.

The two meridional sections, P15 in the west and P16 in the east also show increased warming below $\Theta = 0.8$ °C (Fig. 3a,b). Isotherms slant towards the seafloor in the eastern half the the basin. Thus, there is a higher fraction of AABW in the western half of the basin leading to lower temperatures and increased warming: below 4000 dbar P15 is 0.1 °C colder on average than P16, and warming 90% more per decade.

The N^2 changes along the longitudinal sections (Fig. 3c,d) exhibit more horizontal variability, which can also be observed in $\frac{\partial}{\partial t}\Theta$. Both sections P15 and P16 show a near bottom reduction in N^2, particularly below 5000 dbar. In P15, the strongest N^2 decrease is observed south of 55°S where AABW is advected into the basin, and in the deepest region between 20°S and 35°S (Fig. 3 c). In P16, we observe the most substantial N^2 reduction between 45°S and 35°S.

Averaged across all sections, we find a statistically significant N^2 decrease below $\Theta = 0.75$ °C. Despite variability across isobaths, decadal $\frac{\partial}{\partial t}N^2$ is fairly consistent along isotherm surfaces (Fig. 4). The stratification reduction rate is greater in colder temperature classes at depth. At the AABW boundary ($\Theta = 0.8$ °C) the average factor change is around 0.95, or a 5% percent reduction per decade. In comparison, the $\Theta = 0.63$ °C temperature class has a factor change of 0.71±0.07, which corresponds to a N^2 reduc-

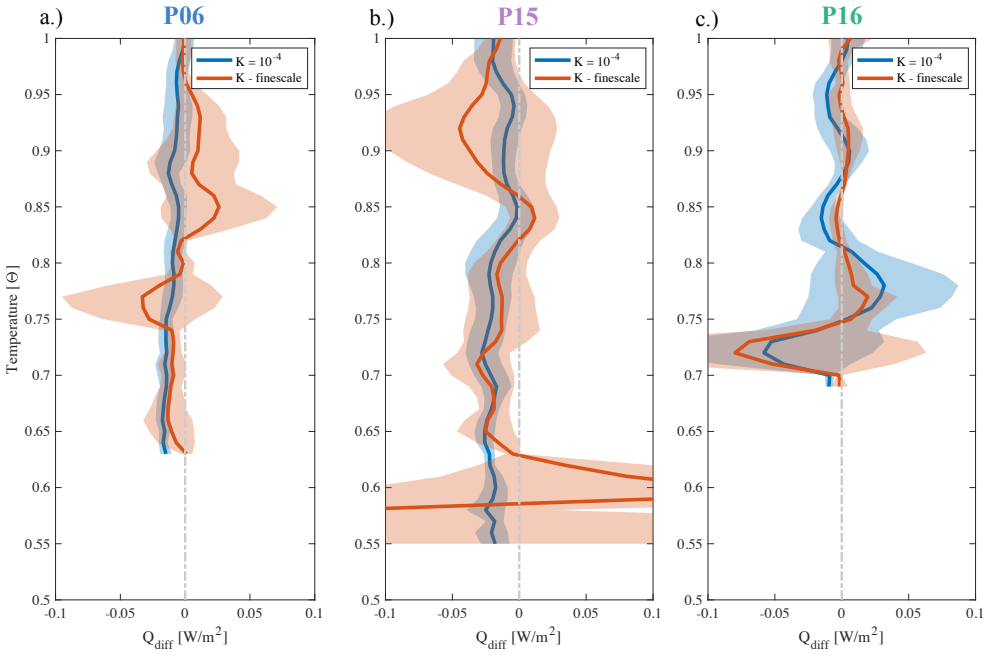

Figure 5. Decadal heat flux change ($\frac{\partial}{\partial t}Q$) for (a) P06 (b) P15 and (c) P16. The blue line represents heat flux calculated using a constant diffusivity of $10^{-4}m^2s^{-1}$ and the orange line represents heat flux calculated using a spatially variable κ based on finescale strain parameterization.

tion of almost 30%. N^2 decrease is observed primarily in the averaged profiles of P06 and P15 (Fig.4b). These two sections contain a significant fraction of AABW, and N^2 is significantly decreasing with good agreement in AABW temperatures down to $\Theta = 0.63$ °C. Below this isotherm, all data comes from a small region at the southern end of P15, leading to greater uncertainty. In contrast, P16 does not show significant N^2 decrease except in DWBC pathway along the base of the East Pacific Rise and therefore samples a smaller fraction of AABW. At and below $\Theta = 0.8$ °C, there is significant spatial variability and the change is not statistically distinguishable from zero until below $\Theta = 0.73$, where the N^2 reduction is comparable with that of P06 and P15.

Similarly, heat flux is also decreasing as a function of time, as approximated from N^2_Θ (Fig.5). Unlike N^2, the trend is calculated linearly, and the change is an absolute value. With a constant diffusivity of $\kappa = 10^{-4}$ m^{2}s^{-1}, the estimated heat flux trend is $\frac{\partial}{\partial t}N^2_\Theta$ scaled by a constant. Using this simplified method, we find an average per decade heat flux reduction of 0.016 ± 0.01 Wm^{-2} below $\Theta = 0.8$ °C. The sections containing

more AABW, P06 and P15, show similar patterns of heat flux reduction, likely associated with the warming of the AABW. Further away from its pathway, there is no significant heat flux reduction in P16 except below $\Theta = 0.70$ °C.

Using a spatially (but not temporally) variable diffusivity estimate (Whalen et al., 2015), the average heat flux reduction below $\Theta = 0.8$ °C is 0.041 ± 0.1 Wm^{-2}. The confidence interval is much wider and the change is not statistically significant. This is due in part to the wide range of diffusivities from 10^{-5} m^{2}s^{-1} in the basin interior up to 10^{-3} m^{2}s^{-1} right above the seafloor (K. Polzin et al., 1997). Despite large confidence intervals in general, there is a significant reduction in a few temperature classes of P06 and in P15 between $\Theta = 0.73$ °C and $\Theta = 0.68$ °C

4 Summary and Discussion

A significant N^2 decrease is observed in the Southwest Pacific Basin for water below $\Theta = 0.8$ °C based on hydrography observations between the 1990s and 2010s. Our analysis agrees with previous results that show a significant warming of AABW along the DWBC in the Southwest Pacific Basin (Sloyan et al., 2013). In addition, we present observations that show that stronger warming at depth leads to a significant reduction of stratification at depth in all three chosen study sections of the Southwest Pacific Basin: P06, P15, and P16.

A consequence of changing stratification is that it alters the medium of internal wave generation, propagation, and dissipation, the main driver of mixing in the deep ocean (St. Laurent & Garrett, 2002; Waterhouse et al., 2014). The energy conversion from barotropic tidal flow over uneven topography to internal gravity waves scales with N (Bell, 1975; Garrett & Kunze, 2007; Melet, Nikurashin, et al., 2013). Once generated, the average energy dissipation rate of internal waves $\langle\epsilon\rangle$ is proportional to N^2 (Gregg, 1989; K. L. Polzin et al., 2014). In the upper ocean, increased surface heating has created a stronger stratification, which is linked to more internal wave activity and turbulent energy dissipation (Capotondi et al., 2012; DeCarlo et al., 2015). In contrast, we find a significant N^2 reduction in near bottom isotherms that is enhanced with depth. Consequently, we expect a decrease in both internal wave tidal energy conversion and turbulent dissipation rate by the respective scaling relations of Bell (1975) and Gregg (1989). Preliminary analysis of tidal energy change shows a statistically insignificant decrease of $(3.64 \pm 8.18) \times$

10^{-4} Wm^{-2} averaged across all three sections in the basin. The wide error interval is a product of low signal to noise ratio and the sensitivity of tidal energy conversion to the topographical variations within the basin (Melet, Nikurashin, et al., 2013). However, recent studies have shown that warming in the Southwest Pacific has accelerated in the 2010s compared to previous decades (Johnson et al., 2019; Purkey et al., 2019). Since we find that N^2 decrease correlates to bottom intensified warming, the accelerated warming may lead to an accelerated N^2 reduction. If this trend continues, the impact on internal waves could become more significant in the coming decades.

In addition to stratification decrease, a weakening temperature gradient results in a smaller downward heat flux. The magnitude of the estimated trend is dependent on whether the diffusivity κ is assumed to be spatially uniform or varying. With uniform diffusivity, the estimated heat flux change is proportional to the changing temperature gradient. Considering the spatial variation of diffusivity accounts for enhanced mixing over rough topography (Ledwell et al., 2000). Since abyssal temperature profiles are relatively homogeneous, a single temperature class may reside in both strong and weak mixing environments, increasing the variance of heat flux change along each Θ value, widening the confidence interval. Heat flux change estimates using both a constant and spatially variable parameterizations of diffusivity show a decreasing trend in downward heat flux over the past three decades. As a result, less heat (and thus buoyancy) is mixed into the deep ocean from above. Over time, this can allow the water column to re-stratify, potentially reversing the observed trend. Additionally, the observed decrease of abyssal heat flux could reduce the ability of the deep ocean to act as a heat sink for the warming upper ocean, although this may be corrected by the negative feedback loop. More research is needed to examine the timescales of these changes and feedbacks, which should be considered both locally and on a global scale.

This study suggests a connection between stratification and heat flux change, which is potentially linked to future changes in internal wave generation and dissipation. Both N^2 and turbulent dissipation are important for upwelling, and an alteration of these terms will have consequences for the strength of the abyssal MOC (Furue & Endoh, 2005; Jayne, 2009; Oka & Niwa, 2013; Hieronymus et al., 2019). However, current efforts have yet to untangle the relative interconnected contributions. While bottom warming is almost ubiquitous in the world's oceans, much is still unknown about stratification change in other basins and how it relates to global mixing processes, heat flux, and ocean circulation.

Since vertical transport of heat and water is key for accurate climate projections (Melet, Hallberg, et al., 2013), more deep ocean research and data, such as the establishment of a Deep Argo program (Johnson et al., 2015), is critical to improving predictions of future climate change.

Acknowledgments

CBW and HJZ were supported by the National Science Foundation Award OCE-1923558 and the University of Washington Royalty Research Fund. SGP was supported by US GO-SHIP (NSF OCE-1437015) and the CLIVAR and Carbon Hydrographic Data Office (NSF OCE 1829814 and NOAA NA15OAR4320071). GO-SHIP CTD hydrography data is publicly available from CCHDO (`https://cchdo.ucsd.edu/`). We are grateful for the PIs, cruise participants, and ship officers and crew who helped collect, calibrate, and process this data.

References

Baines, P. G. (1982). On internal tide generation models. *Deep Sea Research Part A. Oceanographic Research Papers*, *29*(3), 307–338.

Bell, T. (1975). Topographically generated internal waves in the open ocean. *J. Geophys. Res.*, *80*(3), 320–327.

Capotondi, A., Alexander, M. A., Bond, N. A., Curchitser, E. N., & Scott, J. D. (2012). Enhanced upper ocean stratification with climate change in the CMIP3 models. *Journal of Geophysical Research: Oceans*, *117*(C4).

Castagno, P., Capozzi, V., DiTullio, G. R., Falco, P., Fusco, G., Rintoul, S. R., ... Budillon, G. (2019). Rebound of shelf water salinity in the Ross sea. *Nature communications*, *10*(1), 1–6.

DeCarlo, T. M., Karnauskas, K. B., Davis, K. A., & Wong, G. T. (2015). Climate modulates internal wave activity in the Northern South China Sea. *Geophysical Research Letters*, *42*(3), 831–838.

De Lavergne, C., Madec, G., Le Sommer, J., Nurser, A. G., & Naveira Garabato, A. C. (2016). On the consumption of antarctic bottom water in the abyssal ocean. *Journal of Physical Oceanography*, *46*(2), 635–661.

Desbruyères, D., McDonagh, E. L., King, B. A., & Thierry, V. (2017). Global and full-depth ocean temperature trends during the early twenty-first century from

argo and repeat hydrography. *Journal of Climate*, *30*(6), 1985–1997.

Desbruyères, D. G., Purkey, S. G., McDonagh, E. L., Johnson, G. C., & King, B. A. (2016). Deep and abyssal ocean warming from 35 years of repeat hydrography. *Geophysical Research Letters*, *43*(19), 10–356.

Egbert, G., & Ray, R. (2000). Significant dissipation of tidal energy in the deep ocean inferred from satellite altimeter data. *Nature*, *405*(6788), 775–778.

England, M. H. (1995). The age of water and ventilation timescales in a global ocean model. *Journal of Physical Oceanography*, *25*(11), 2756–2777.

Furue, R., & Endoh, M. (2005). Effects of the Pacific diapycnal mixing and wind stress on the global and Pacific meridional overturning circulation. *Journal of physical oceanography*, *35*(10), 1876–1890.

Garrett, C., & Kunze, E. (2007). Internal tide generation in the deep ocean. *Annu. Rev. Fluid Mech.*, *39*, 57–87.

Gregg, M. (1989). Scaling turbulent dissipation in the thermocline. *Journal of Geophysical Research: Oceans*, *94*(C7), 9686–9698.

Gurvich, A., & Yaglom, A. (1967). Breakdown of eddies and probability distributions for small-scale turbulence. *The Physics of Fluids*, *10*(9), S59–S65.

Hieronymus, M., Nycander, J., Nilsson, J., Döös, K., & Hallberg, R. (2019). Oceanic overturning and heat transport: The role of background diffusivity. *Journal of Climate*, *32*(3), 701–716.

Hood, E., Sabine, C., & Sloyan, B. (2010). GO-SHIP Repeat Hydrography Manual, Version 1: Cover page and contents.

Jacobs, S. S., & Giulivi, C. F. (2010). Large multidecadal salinity trends near the Pacific–Antarctic continental margin. *Journal of Climate*, *23*(17), 4508–4524.

Jayne, S. R. (2009). The impact of abyssal mixing parameterizations in an ocean general circulation model. *Journal of Physical Oceanography*, *39*(7), 1756–1775.

Johnson, G. C. (2008). Quantifying Antarctic bottom water and North Atlantic deep water volumes. *Journal of Geophysical Research: Oceans*, *113*(C5).

Johnson, G. C., Lyman, J. M., & Purkey, S. G. (2015). Informing deep argo array design using argo and full-depth hydrographic section data. *Journal of Atmospheric and Oceanic Technology*, *32*(11), 2187–2198.

Johnson, G. C., Mecking, S., & Sloyan, S. E., BernadeWijffels. (2007). Recent bot-

tom water warming in the Pacific Ocean. *Journal of Climate*, *20*(21), 5365–5375.

Johnson, G. C., Purkey, S. G., & Toole, J. M. (2008). Reduced antarctic meridional overturning circulation reaches the north atlantic ocean. *Geophysical Research Letters*, *35*(22).

Johnson, G. C., Purkey, S. G., Zilberman, N. V., & Roemmich, D. (2019). Deep Argo quantifies bottom water warming rates in the southwest Pacific Basin. *Geophysical Research Letters*, *46*(5), 2662–2669.

Kawano, T., Aoyama, M., Joyce, T., Uchida, H., Takatsuki, Y., & Fukasawa, M. (2006). The latest batch-to-batch difference table of standard seawater and its application to the WOCE onetime sections. *Journal of oceanography*, *62*(6), 777–792.

Kouketsu, S., Doi, T., Kawano, T., Masuda, S., Sugiura, N., Sasaki, Y., ... others (2011). Deep ocean heat content changes estimated from observation and reanalysis product and their influence on sea level change. *Journal of Geophysical Research: Oceans*, *116*(C3).

Kouketsu, S., Fukasawa, M., Kaneko, I., Kawano, T., Uchida, H., Doi, T., ... Murakami, K. (2009). Changes in water properties and transports along 24 n in the north pacific between 1985 and 2005. *Journal of Geophysical Research: Oceans*, *114*(C1).

Ledwell, J., Montgomery, E., Polzin, K., Laurent, L. S., Schmitt, R., & Toole, J. (2000). Evidence for enhanced mixing over rough topography in the abyssal ocean. *Nature*, *403*(6766), 179–182.

Lumpkin, R., & Speer, K. (2007). Global ocean meridional overturning. *Journal of Physical Oceanography*, *37*(10), 2550–2562.

Masuda, S., Awaji, T., Sugiura, N., Matthews, J. P., Toyoda, T., Kawai, Y., ... others (2010). Simulated rapid warming of abyssal North Pacific waters. *Science*, *329*(5989), 319–322.

McDougall, T. J., & Barker, P. M. (2011). Getting started with TEOS-10 and the Gibbs Seawater (GSW) oceanographic toolbox. *SCOR/IAPSO WG*, *127*, 1–28.

Melet, A., Hallberg, R., Legg, S., & Nikurashin, M. (2014). Sensitivity of the ocean state to lee wave–driven mixing. *Journal of physical oceanography*, *44*(3), 900–

921.

Melet, A., Hallberg, R., Legg, S., & Polzin, K. (2013). Sensitivity of the ocean state to the vertical distribution of internal-tide-driven mixing. *Journal of Physical Oceanography*, *43*(3), 602–615.

Melet, A., Nikurashin, M., Muller, C., Falahat, S., Nycander, J., Timko, P. G., ... Goff, J. A. (2013). Internal tide generation by abyssal hills using analytical theory. *Journal of Geophysical Research: Oceans*, *118*(11), 6303–6318.

Munk, W. H. (1966). Abyssal recipes. In *Deep sea research and oceanographic abstracts* (Vol. 13, pp. 707–730).

Nikurashin, M., & Ferrari, R. (2013). Overturning circulation driven by breaking internal waves in the deep ocean. *Geophysical Research Letters*, *40*(12), 3133–3137.

Oka, A., & Niwa, Y. (2013). Pacific deep circulation and ventilation controlled by tidal mixing away from the sea bottom. *Nature communications*, *4*(1), 1–8.

Orsi, A. H., Johnson, G. C., & Bullister, J. L. (1999). Circulation, mixing, and production of Antarctic Bottom Water. *Progress in Oceanography*, *43*(1), 55–109.

Polzin, K., Toole, J., Ledwell, J., & Schmitt, R. (1997). Spatial variability of turbulent mixing in the abyssal ocean. *Science*, *276*(5309), 93–96.

Polzin, K. L., Garabato, A. C. N., Huussen, T. N., Sloyan, B. M., & Waterman, S. (2014). Finescale parameterizations of turbulent dissipation. *Journal of Geophysical Research: Oceans*, *119*(2), 1383–1419.

Polzin, K. L., Toole, J. M., & Schmitt, R. W. (1995). Finescale parameterizations of turbulent dissipation. *Journal of physical oceanography*, *25*(3), 306–328.

Purkey, S. G., & Johnson, G. C. (2010). Warming of global abyssal and deep Southern Ocean waters between the 1990s and 2000s: Contributions to global heat and sea level rise budgets. *Journal of Climate*, *23*(23), 6336–6351.

Purkey, S. G., & Johnson, G. C. (2012). Global contraction of Antarctic Bottom Water between the 1980s and 2000s. *Journal of Climate*, *25*(17), 5830–5844.

Purkey, S. G., & Johnson, G. C. (2013). Antarctic Bottom Water warming and freshening: Contributions to sea level rise, ocean freshwater budgets, and global heat gain. *Journal of Climate*, *26*(16), 6105–6122.

Purkey, S. G., Johnson, G. C., Talley, L. D., Sloyan, B. M., Wijffels, S. E., Smethie, W., ... Katsumata, K. (2019). Unabated Bottom Water Warming and Fresh-

455 ening in the South Pacific Ocean. *Journal of Geophysical Research: Oceans*,
456 *124*(3), 1778-1794. doi: 10.1029/2018JC014775

457 Rignot, E., Mouginot, J., Scheuchl, B., van den Broeke, M., van Wessem, M. J.,
458 & Morlighem, M. (2019). Four decades of antarctic ice sheet mass balance
459 from 1979–2017. *Proceedings of the National Academy of Sciences*, *116*(4),
460 1095–1103.

461 Roemmich, D., Hautala, S., & Rudnick, D. (1996). Northward abyssal transport
462 through the Samoan Passage and adjacent regions. *Journal of Geophysical Re-*
463 *search: Oceans*, *101*(C6), 14039–14055.

464 Roquet, F., Madec, G., McDougall, T. J., & Barker, P. M. (2015). Accurate poly-
465 nomial expressions for the density and specific volume of seawater using the
466 teos-10 standard. *Ocean Modelling*, *90*, 29–43.

467 Sloyan, B. M., & Rintoul, S. R. (2001). The southern ocean limb of the global deep
468 overturning circulation. *Journal of Physical Oceanography*, *31*(1), 143–173.

469 Sloyan, B. M., Wijffels, S. E., Tilbrook, B., Katsumata, K., Murata, A., & Mac-
470 donald, A. M. (2013). Deep ocean changes near the western boundary of the
471 South Pacific Ocean. *Journal of physical oceanography*, *43*(10), 2132–2141.

472 St. Laurent, L., & Garrett, C. (2002). The role of internal tides in mixing the deep
473 ocean. *Journal of Physical Oceanography*, *32*(10), 2882–2899.

474 St. Laurent, L., & Simmons, H. (2006). Estimates of power consumed by mixing in
475 the ocean interior. *Journal of climate*, *19*(19), 4877–4890.

476 Talley, L. D. (2013). Closure of the global overturning circulation through the In-
477 dian, Pacific, and Southern Oceans: Schematics and transports. *Oceanography*,
478 *26*(1), 80–97.

479 Talley, L. D., Reid, J. L., & Robbins, P. E. (2003). Data-based meridional over-
480 turning streamfunctions for the global ocean. *Journal of Climate*, *16*(19),
481 3213–3226.

482 Voet, G., Alford, M. H., Girton, J. B., Carter, G. S., Mickett, J. B., & Klymak,
483 J. M. (2016). Warming and weakening of the abyssal flow through Samoan
484 Passage. *Journal of Physical Oceanography*, *46*(8), 2389–2401.

485 Waterhouse, A. F., MacKinnon, J. A., Nash, J. D., Alford, M. H., Kunze, E., Sim-
486 mons, H. L., ... Lee, C. M. (2014). Global patterns of diapycnal mixing from
487 measurements of the turbulent dissipation rate. *J. Phys. Oceanogr.*, 1854-1872.

488 doi: 10.1175/JPO-D-13-0104.1

489 Whalen, C. B., MacKinnon, J. A., Talley, L. D., & Waterhouse, A. F. (2015). Es-
490 timating the mean diapycnal mixing using a finescale strain parameterization.
491 *Journal of Physical Oceanography*, *45*(4), 1174–1188.

492 Whitworth, T., Warren, B., Nowlin Jr, W., Rutz, S., Pillsbury, R., & Moore, M.
493 (1999). On the deep western-boundary current in the Southwest Pacific Basin.
494 *Progress in Oceanography*, *43*(1), 1–54.